AIAA'86

AIAA-86-0542

A new method for stability analysis of a free jet with arbitrary cross section.

S. Koshigoe, Naval Weapons Center, China Lake, CA; V. Yang and F.E.C. Culick, California Institute of Technology, Pasadena, CA; and A. Tubis, Purdue University, West Lafayette, IN.

AIAA 24th Aerospace Sciences Meeting
January 6-9, 1986/Reno, Nevada

A NEW METHOD FOR STABILITY ANALYSIS OF A FREE JET WITH ARBITRARY CROSS SECTION

S. Koshigoe
Naval Weapons Center
China Lake, California
and
V. Yang and F. E. C. Culick
California Institute of Technology
Pasadena, California
and
A. Tubis
Purdue University
West Lafayette, Indiana

Abstract

A new approach for linear analysis of the stability of jets with arbitrary mean velocity profiles is presented. This method is based on utilizing Green function techniques to transform the Rayleigh equation into an integral equation form. The integral equation is then solved numerically using a type of finite element approximation to determine the eigenvectors and complex wave numbers of various instability modes. In order to demonstrate this method's capability of handling arbitrary jet mean velocity profiles, a comparison is made to the elliptic jet case where generally good agreement is apparent[1].

A brief discussion on how the effects of compressibility and temperature variation in flows can be incorporated within the formalism is presented.

1. Introduction

In recent years the large-scale turbulent structures of a free jet has been studied intensively in connection with the control of mixing layers and the mechanism of noise generation. The existence of these structures of a jet were first reported by Mollo-Christensen[2], and then by a number of other investigators[3-4]. The gross statistical description of these large-scale turbulent structures of a jet can be reliably predicted by assuming that they are associated with instability waves of a mean flow profile[5-7], and that spatial growth rates of these waves may be estimated from Rayleigh linear inviscid instability analysis. Previous studies in this area have been concerned with plane jet shear layers and simple jet cross sections. Recent experimental interest on non-circular jets[8-12] has, to date, prompted only a few related analyses of the Rayleigh equation. Crighton considered the vortex sheet elliptical jet and Morris and Miller analyzed several instability modes of elliptical jets with shear layers described by both vortex sheet and continuous velocity profiles. These authors formulated the Rayleigh equation in the natural coordinate system for the problem.

The aim of the present work is to develop formalism which can be applied to the linear analysis of jet stability in the cases where the mean velocity profiles are arbitrary. The general formalism will be described in section 2, and applied for analysis of elliptic jet stability (as an example demonstration) in section 3. Some of the calculation results will be compared with Morris and Miller's results in section 4. For the purpose of comparison, the flow will be assumed to be incompressible and isothermal, and the influence of divergent flow as considered by Crighton and Gaster[14] and viscous effects by Morris[15] will be ignored.

2. General Formulation

In order to discuss the flow field in a jet with an arbitrary mean velocity profile, the cartesian coordinate system shown in Figure 1 is used. The z-axis points in the direction of the jet axis, and the jet nozzle plane is located in the x-y plane. The usual assumptions that: (1) the undisturbed free jet can be considered as a parallel flow and only has an axial velocity component, and (2) the viscous effects on the stability of the jet are negligible, are followed.

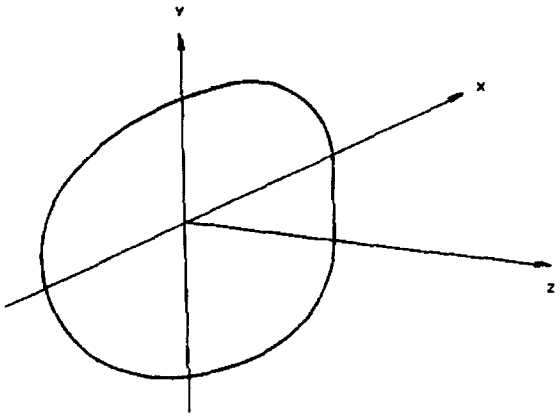

Figure. 1. Coordinate System for a Jet With Arbitrary Linear Velocity Profile.

The temperature variation in the undisturbed jet $T(\vec{x})$ is related to the undisturbed jet velocity profile $W(\vec{x})$ as in the boundary layer[6]. In that case Busemann-Crocco's relationship is expressed as:

$$T(\vec{x}) = To\left[Tr + (1 - Tr)\frac{W(\vec{x})}{Wo} + \frac{\gamma - 1}{2} Mo^2 \frac{W(\vec{x})}{Wo}\left(1 - \frac{W(\vec{x})}{Wo}\right)\right], \qquad (2\text{-}1)$$

where $To = T(|\vec{x}| = 0)$, $T_1 = T(|\vec{x}| = \infty)$, $Tr = T_1/To$, $Wo = W(|\vec{x}| = 0)$, $Mo = Wo/ao$, $ao = a(|\vec{x}| = 0)$, and $a(\vec{x})$ is the local sound speed which is related to the temperature as:

$$a(\vec{x}) = ao\sqrt{T(\vec{x})/To} \qquad (2\text{-}2)$$

The governing equations for the mass, momentum, and energy are given by:

$$\frac{\partial \rho}{\partial t} + \vec{\nabla} \cdot (\rho \vec{U}) = 0,$$

$$\rho \frac{\partial \vec{U}}{\partial t} + \rho \vec{U} \cdot \vec{\nabla} \vec{U} + \vec{\nabla} p = 0, \qquad (2\text{-}3)$$

and

$$\frac{p}{p_o} = \left(\frac{\rho}{\rho_o}\right)^{\gamma},$$

where

$$\vec{\nabla} = \sum_{i=1}^{3} \vec{e}_i \frac{\partial}{\partial x_i}$$

Total pressure, density, and velocity fields may then be decomposed into time averaged and perturbation parts giving:

$$p = p_o + p$$

$$\rho = \rho_o + \rho \qquad (2\text{-}4)$$

and $\vec{U} = W(\vec{x})\, \vec{e}_z + \vec{u}$.

Since the analysis is linear, the perturbation terms for p, ρ, and $\vec{u}$ are assumed to have z and t dependencies as $\exp\left(i(\alpha z - \omega t)\right)$.

After substitution of eq. (2-4) and use of the z and t dependencies for p, ρ, and $\vec{u}$ in the eq. (2-3), collecting the linear terms results in:

$$(\vec{\nabla}^2 - \tilde{\alpha}_c^2)\, p = -\frac{2\alpha}{\omega - \alpha W} \vec{\nabla} W \cdot \vec{\nabla} p, \qquad (2\text{-}5)$$

where

$$\tilde{\alpha}_c^2 = \alpha^2 \left\{ 1 - \left(\frac{\omega/\alpha - W}{a(\vec{x})} \right)^2 \right\},$$

and

$$\vec{\nabla} = \sum_{i=1}^{2} \vec{e}_i \frac{\partial}{\partial x_i}$$

It is reasonable to assume that the variation of the $W(\vec{x})$ is approximately confined to the momentum thickness schematically shown in Figure 2. The computation domains are also shown in Figure 2 and may be divided into two parts. Domain (0) is represented by the shaded area, and domain (1) consists of the remainder of the x-y plane. In domain (0), eq. 2-5 is expressed as:

$$(\vec{\nabla} - \tilde{\alpha}_c^2)\, p_{(0)} = 0, \qquad (2\text{-}6)$$

where

$$\tilde{\alpha}_c^2 = \alpha^2 \left\{ 1 - \left(\frac{\omega/\alpha - W_o}{a_o} \right)^2 \right\} \text{ is constant.}$$

In domain (1), eq. (2-5) becomes:

$$(\vec{\nabla}^2 - \alpha^2)\, p_{(1)} = f_{(1)}, \qquad (2\text{-}7)$$

where

$$f_{(1)} = -\frac{2\alpha}{\omega - \alpha W} \vec{\nabla} W \cdot \vec{\nabla} p - \left(\frac{\omega - \alpha W}{a} \right)^2 p.$$

Now, two free space Green functions may be introduced:

$$G_{(0)}(\vec{x}|\vec{x}') = i\pi H_0^{(1)}(i\tilde{\alpha}_c |\vec{x} - \vec{x}'|) \qquad (2\text{-}8)$$

in domain (0), and

$$G_{(0)}(\vec{x}|\vec{x}') = i\pi H_0^{(1)}(i\alpha |\vec{x} - \vec{x}'|) \qquad (2\text{-}9)$$

domain (1), where $H_0^{(1)}$ is the Hankel function.

These Green functions are solutions of:

$$(\vec{\nabla}^2 - \tilde{\alpha}_c^2)\, G_{(0)}(\vec{x}|\vec{x}') = -\delta(\vec{x} - \vec{x}'),$$

$$(\vec{\nabla}^2 - \alpha^2)\, G_{(1)}(\vec{x}|\vec{x}') = -\delta(\vec{x} - \vec{x}'),$$

respectively.

Using Green's theorem, eq. (2-6) may be expressed in the line integral equation form as:

$$p_{(0)}(\vec{x}) = \int_{\text{boundary}} \left(G_{(0)}(\vec{x}|\vec{\xi}') \frac{\partial p_{(0)}(\vec{\xi}')}{\partial n''} - p_{(0)}(\vec{\xi}') \frac{\partial G_{(0)}(\vec{x}|\vec{\xi}')}{\partial n''} \right) d\xi',$$

where the line integral covers the boundary between domain (0) and domain (1), and where n'' represents the unit vector points the outward normal from domain (0). As $\vec{x}$ is approached $\vec{\xi}$ which is on the boundary, the above expression becomes:

$$p_{(1)}(\vec{\xi}) = \int_{\text{boundary}} \left(p_{(1)}(\vec{\xi}') \frac{\partial G_{(0)}(\vec{\xi}|\vec{\xi}')}{\partial n'} - G_{(0)}(\vec{\xi}|\vec{\xi}') \frac{\partial p_{(1)}(\vec{\xi}')}{\partial n'} \right) d\xi', \qquad (2\text{-}10)$$

where n' represents the outward normal unit vector from domain(1), and the continuities of $p(\vec{x})$ and its derivative at the boundary are used.

Similarly, eq. (2-7) may be written in the integral equation form as:

$$p_{(1)}(\vec{x}) = -\int G_{(1)}(\vec{x}|\vec{x}')\, f_{(1)}(\vec{x}')\, ds' + \int_{\text{boundary}} \left(G_{(1)}(\vec{x}|\vec{\xi}') \frac{\partial p_{(1)}(\vec{\xi}')}{\partial n'} - p_{(1)}(\vec{\xi}') \frac{\partial G(\vec{x}|\vec{\xi}')}{\partial n'} \right) d\ell', \quad (2\text{-}11)$$

where the surface integral (the first term) is bounded on the dotted area if Figure 2. These integral equations are discretized by using a type of finite element approximation[16]. Elimination of the $\partial p_{(1)}(\vec{\xi})/\partial n'$ from eq. (2-11) are achieved through the use of eq. (2-10). The final discretized form of eq. (2-11) is then:

$$A(\alpha, W)\, \hat{P} = 0 \quad (2\text{-}12)$$

Thus, given $W(\vec{x})$ and ω, one may determine the eigenvalues α and the corresponding eigenvectors $\hat{p}$.

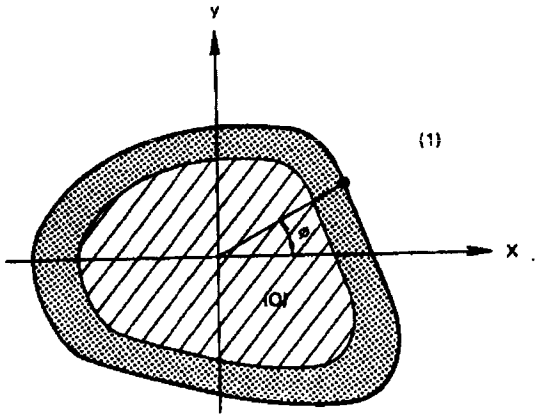

Figure 2. Schematic Representation of Non-Zero Variation Area for $W(\vec{x})$ (dotted area) and the computation Domains (0) and (1).

3. An Example Application (Elliptic Jet)

Here the general formulas developed in section 2 are applied for analysis of elliptic jet stability.

Since the flow is assumed to be incompressible ($a(\vec{x}) = \infty$) in this case, the previously obtained equations are simplified as follows. The complex wave number α_c in eq. 2-5) becomes a constant α, and therefore, the corresponding integral equation is expressed as:

$$p(\vec{x}) = \frac{\alpha}{2\pi} \int d\vec{x}' \frac{G(\vec{x}|\vec{x}')}{\omega - \alpha W(\vec{x})} \vec{\nabla}' W(\vec{x}') \cdot \vec{\nabla}' p(\vec{x}'), \quad (3\text{-}1)$$

where the Green function $G(\vec{x}|\vec{x}')$ is the same as $G_{(0)}(\vec{x}|\vec{x}')$ in eq. (2-8). In the actual calculation, eq. (3-1) is rearranged as:

$$\frac{\alpha}{2\pi} \frac{\nabla W(\vec{x})}{\omega - \alpha W(\vec{x})} \int d\vec{x}' \vec{\nabla} G(\vec{x}|\vec{x}')\, S(\vec{x}') - S(\vec{x}) = 0, \quad (3\text{-}2)$$

where:

$$S(\vec{x}) = \frac{\nabla W(\vec{x}) \cdot \nabla p(\vec{x})}{\omega - \alpha W(\vec{x})}$$

The surface integration is done over the narrow region where $W(\vec{x})$ is non-zero.

The size of the integration is further reduced by the two symmetries involved in the mean velocity profile $W(\vec{x})$, which are;

$$W(\pi - \phi) = W(\phi) \quad (3\text{-}3)$$
$$W(\phi + \pi) = W(\phi)$$

(see Figure 2). Knowing that the ϕ dependency of the kernel of the integral (eq. (3-2)) is the difference, $\phi - \phi'$, it follows that the use of eq. (3-3) leads to the symmetries:

$$S(\pi - \phi) = \pm S(\phi) \quad (3\text{-}4)$$
$$S(\phi + \pi) = \pm S(\phi)$$

in the eigenvectors. They constitute four classes of solutions (++, +−, −+, −−) as shown in Figure 3.

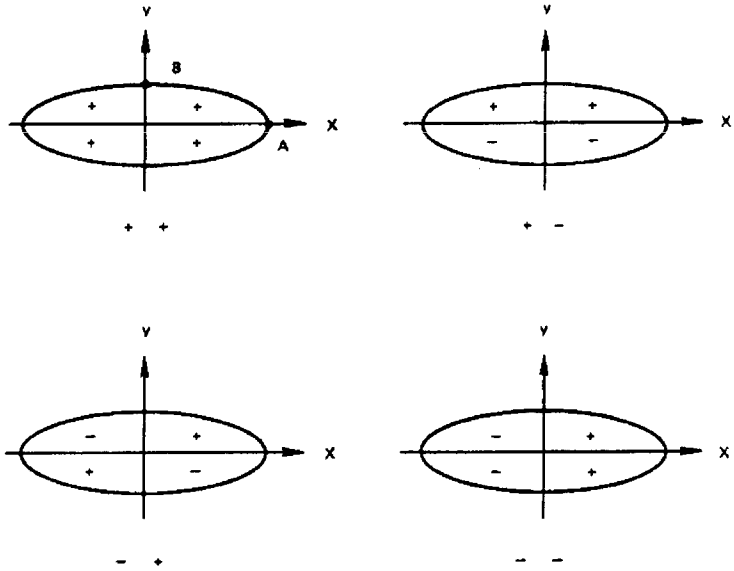

Figure 3. Four Classes of Solution for the Elliptic Jet Corresponding to $\{\cos 2n\phi\}$, $\{\sin(2n+1)\phi\}$, $\{\sin(2n+2)\phi\}$, and $\{\cos(2n+1)\phi\}$, where n = 0, 1, . . . for the circular jet.

Now, the domain of the surface integral in eq. (3-2) is just over the narrow non-zero $W(\vec{x})$ region in the first quadrant. The discretization of eq. (3-2) is carried out through the following approximations: (1) the integration domain is divided into nine node quadratic elements, (2) on each element the eigenvectors are interpolated linearly, and (3) the nine points Gaussian quadrature is used for the numerical integration. The final discretized form is similar to eq. (2-12), and the α roots of det A $(\alpha, \omega) = 0$ are found through the use of Newton's method.

4. Calculation Results

In the following, some of the calculation results will be compared with Morris and Miller's

elliptic jet calculations. All the variable are non-dimensionalized through the length of the semi-major axis A and the center mean velocity W_o. For the mean velocity profile, the same expression as used by Morris and Miller is utilized. It is:

$$W(\rho)=\frac{1}{2}[1+\tanh\left\{\frac{B}{2\theta_B}(1-\sinh\rho/\sinh\rho_0)\right\}] \quad (4\text{-}1)$$

where B is the length of the semi-minor axis,

$$\rho_0=\frac{1}{2}\ln\left\{(A/B+1)/(A/B-1)\right\},$$

$$\frac{B}{2\theta_B}=\left\{\frac{1}{2\theta_A}(A/B)^{-3/2}\right\}$$

$$\theta_A = 0.02,$$

and ρ is one of the elliptic coordinates.

These are related to x and y by:

$$x = \cosh\rho\cos\theta/\cosh\rho_0$$

and $y = \sinh\rho\sin\theta/\cosh\rho_0$.

The node points (square boxes) for the quadratic elements which cover the non-zero variation area for $W(\vec{x})$ are shown in Figure 4.

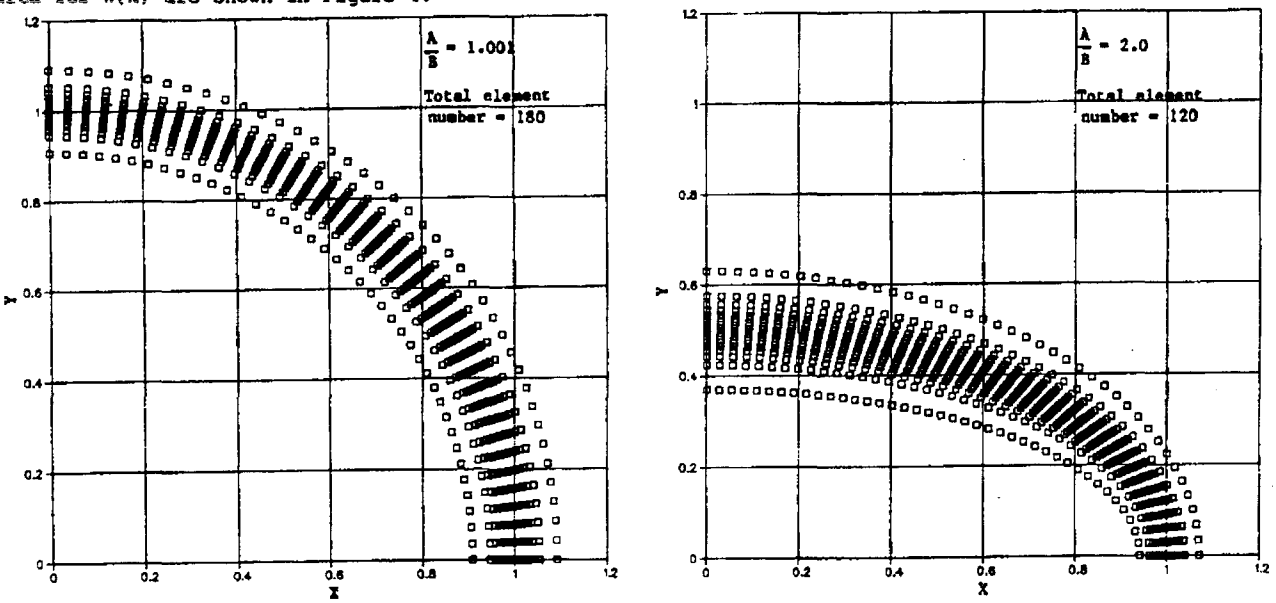

Figure 4. Node Points for the Quadratic Elements.

In Figure 5, the axial wave numbers α_r and the growth rates α_i of the lowest mode in the ++ case are shown as functions of ω for various A/B. These calculated values are essentially the same as the results of Morris and Miller, thus showing that the mode becomes more stable as eccentricity is increased.

In Figure 6, similar relations are depicted for the +− case. The calculation results for A/B=1.001) show good agreement, however, the larger eccentricity case of A/B=2.0 displays a substantial difference in the higher frequency behaviors. If the higher modes, rather than the lowest ones are used in the high frequency region, then the results are in good agreement with those of Morris and Miller.

In order to verify $\alpha_r(\omega)$ and $\alpha_i(\omega)$, the test of applying the disperson relations on them[17-20] is being undertaken in a separate effort.

Figure 7 shows the eigenvalues α (represented by circles) corresponding to the lowest three modes in the ++ case at the frequency $\omega = 5.4$ with (a) A/B=1.001 and (b) A/B=2.0. The initial guesses for α are indicated by the dots. The phase variations of the eigenvectors corresponding to these eigenvalues are shown in Figures 8 and 9. In these figures, the solid and dotted lines represent positive and negative phase portions, respectively. It is clear from these figures that when the eccentricity is small, the change in the phase variations are quite orderly as the mode shifts from the lowest to the higher ones. On the other hand, when the eccentricity is increased, the behaviors are much more complex. Also, it is apparent that the mode becomes more stable as it shifts higher.

These same findings are true for the +− case, as shown on the next three figures (Figures 10-12).

Finally, a comparison of Figures 7 and 10 shows that all three modes of the +− case are more stable than those of the ++ case when the eccentricity is small. However, this situation reverses when the eccentricity is increased.

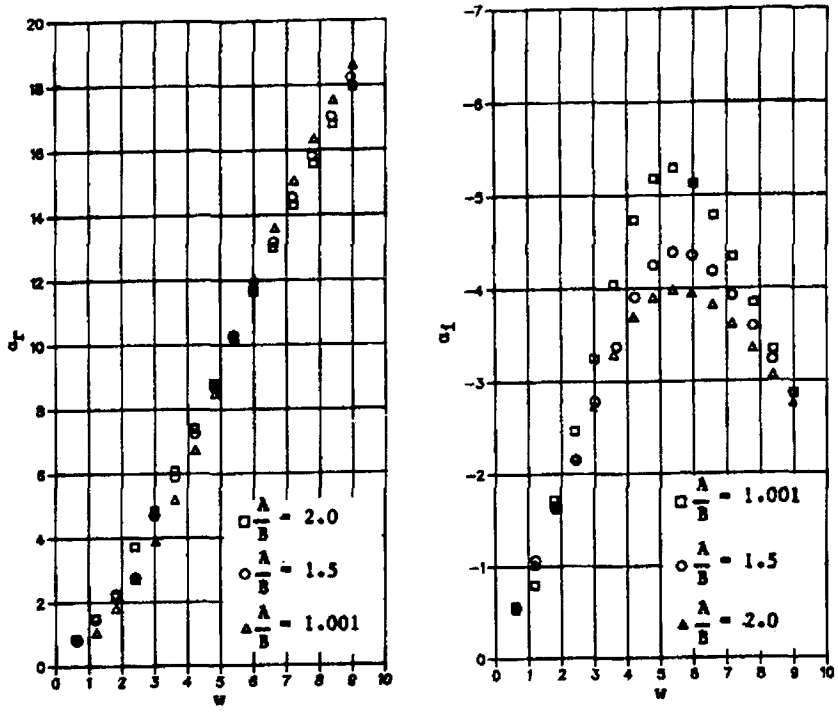

(a) (b)

Figure 5. Axial Wave Numbers α_r (a) and Growth Rates α_i (b) of the Lowest Mode for the ++ Case.

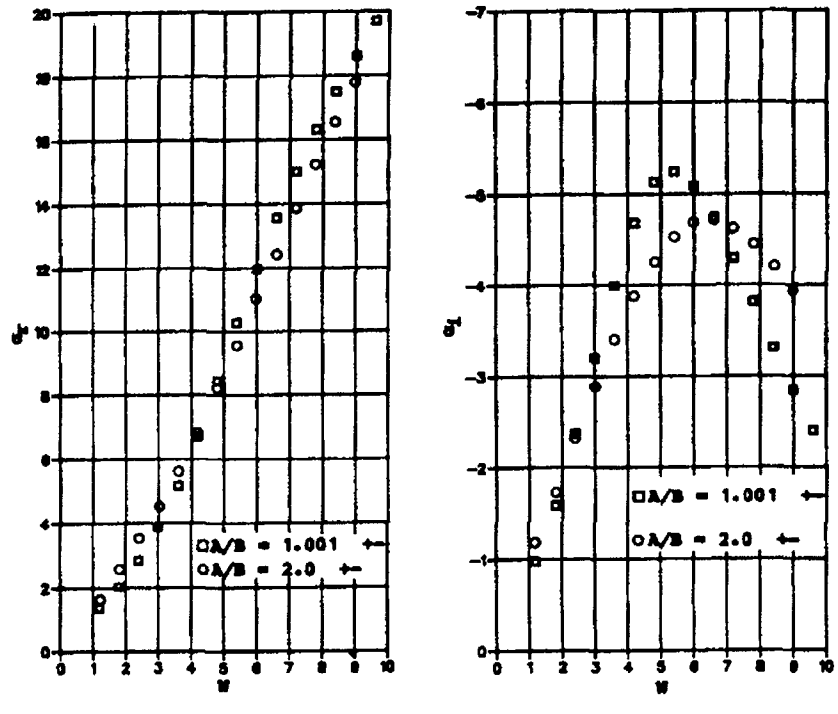

(a) (b)

Figure 6. Axial Wave Numbers α_r (a) and Growth Rates α_i (b) of the Lowest Mode for the ++ Case.

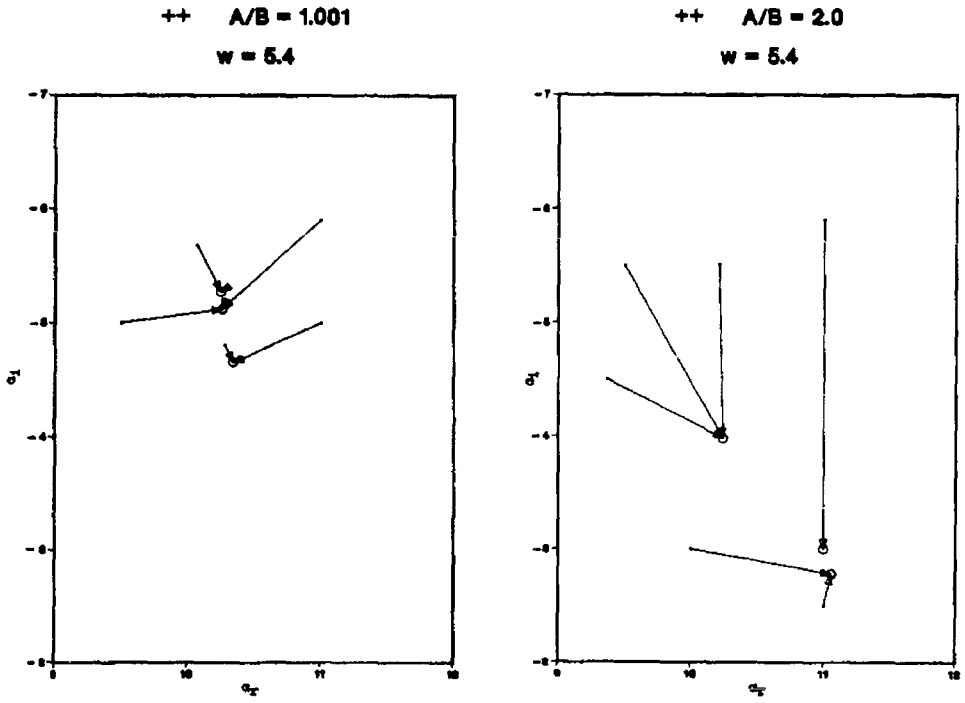

Figure 7. Eignevalues α corresponding to the lowest three modes (++ case).

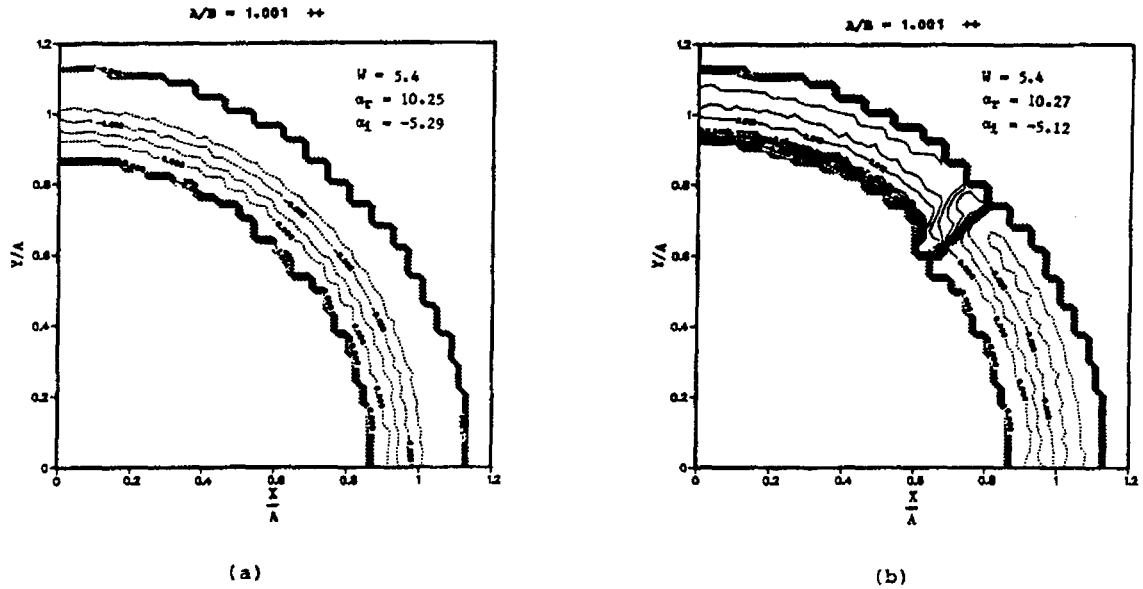

Figure 8. Phase Variations of the Eigenvectors Corresponding to the Eigenvalues in Figure 7(a) (dotted line = negative, solid line = positive).

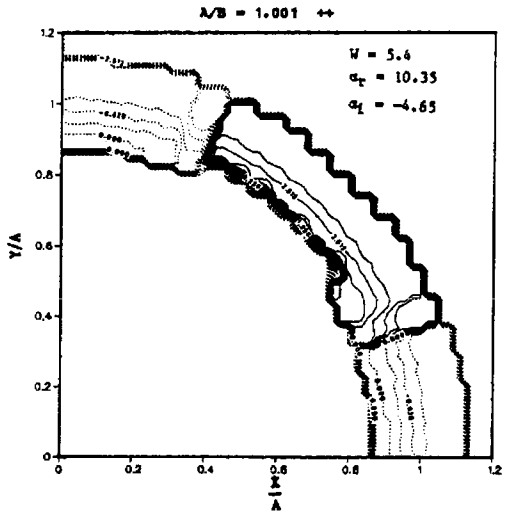

(c)

Figure 8 (Cont.)

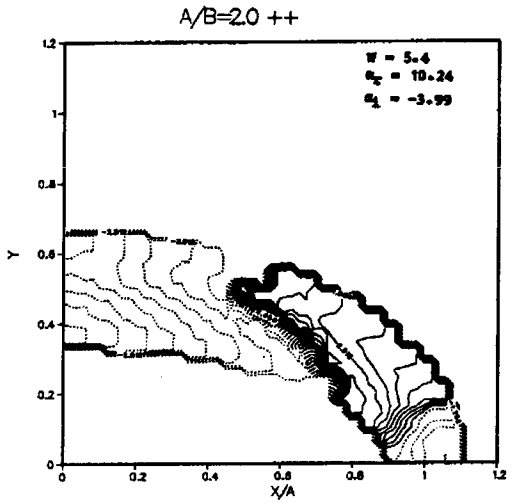

(a)

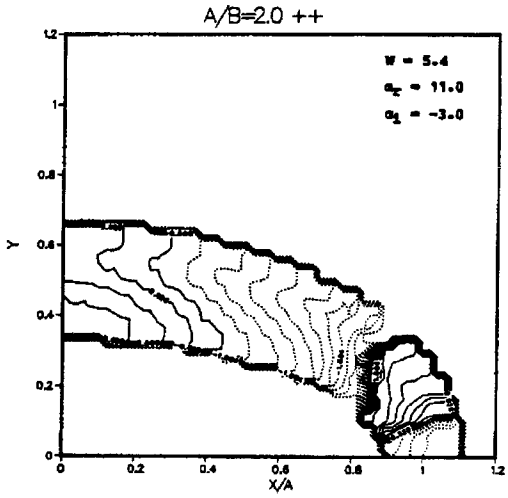

(b)

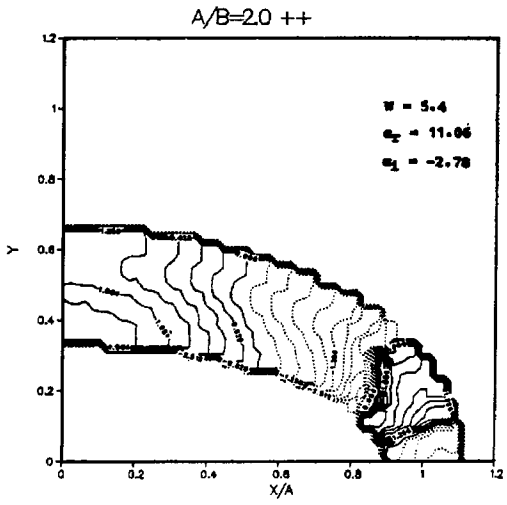

(c)

Figure 9. Phase Variations of the Eigenvectors Corresponding to the Eigenvalues in Figure 7(b) (dotted line = negative, solid line = positive).

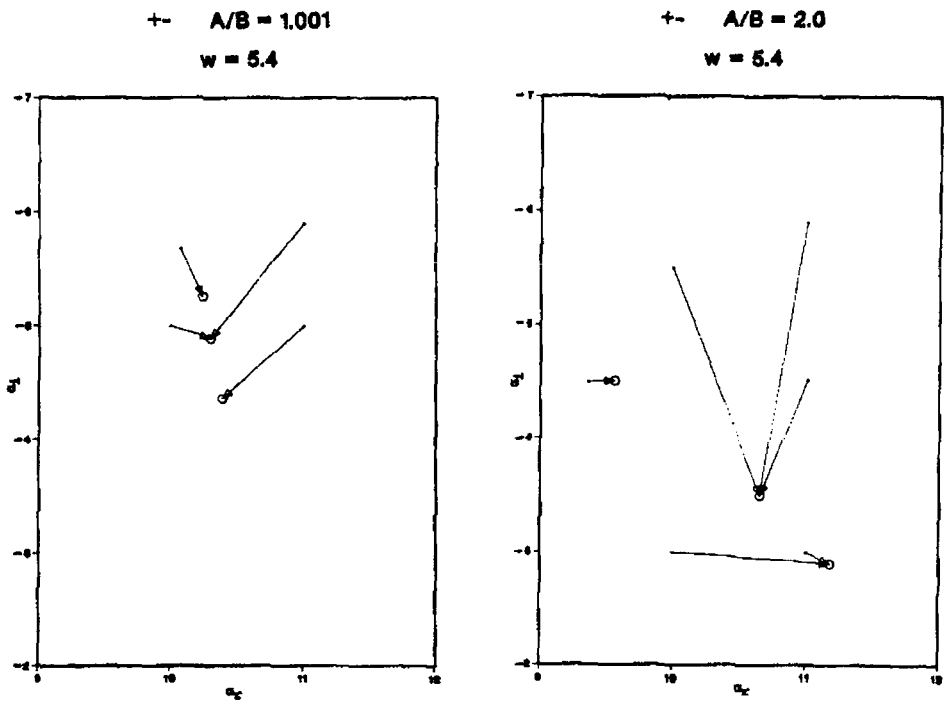

Figure 10. Eigenvalues α Corresponding to the Lowest Three Modes (+- case).

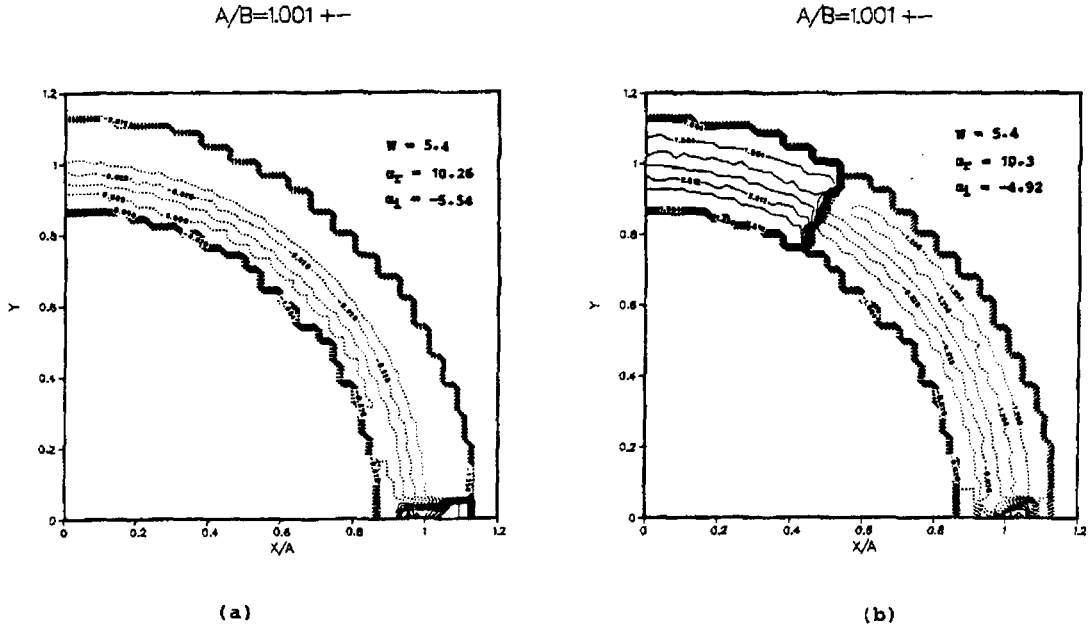

Figure 11. Phase Variations of the Eigenvectors Corresponding to the Eigenvalues in Figure 10(a) (dotted line = negative, solid line = positive).

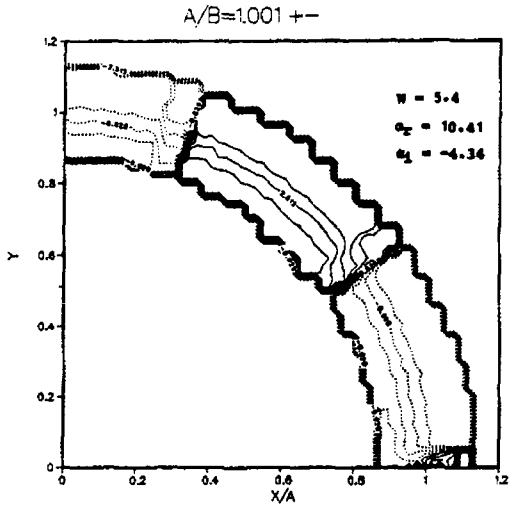

(c)

Figure 11 (Cont.)

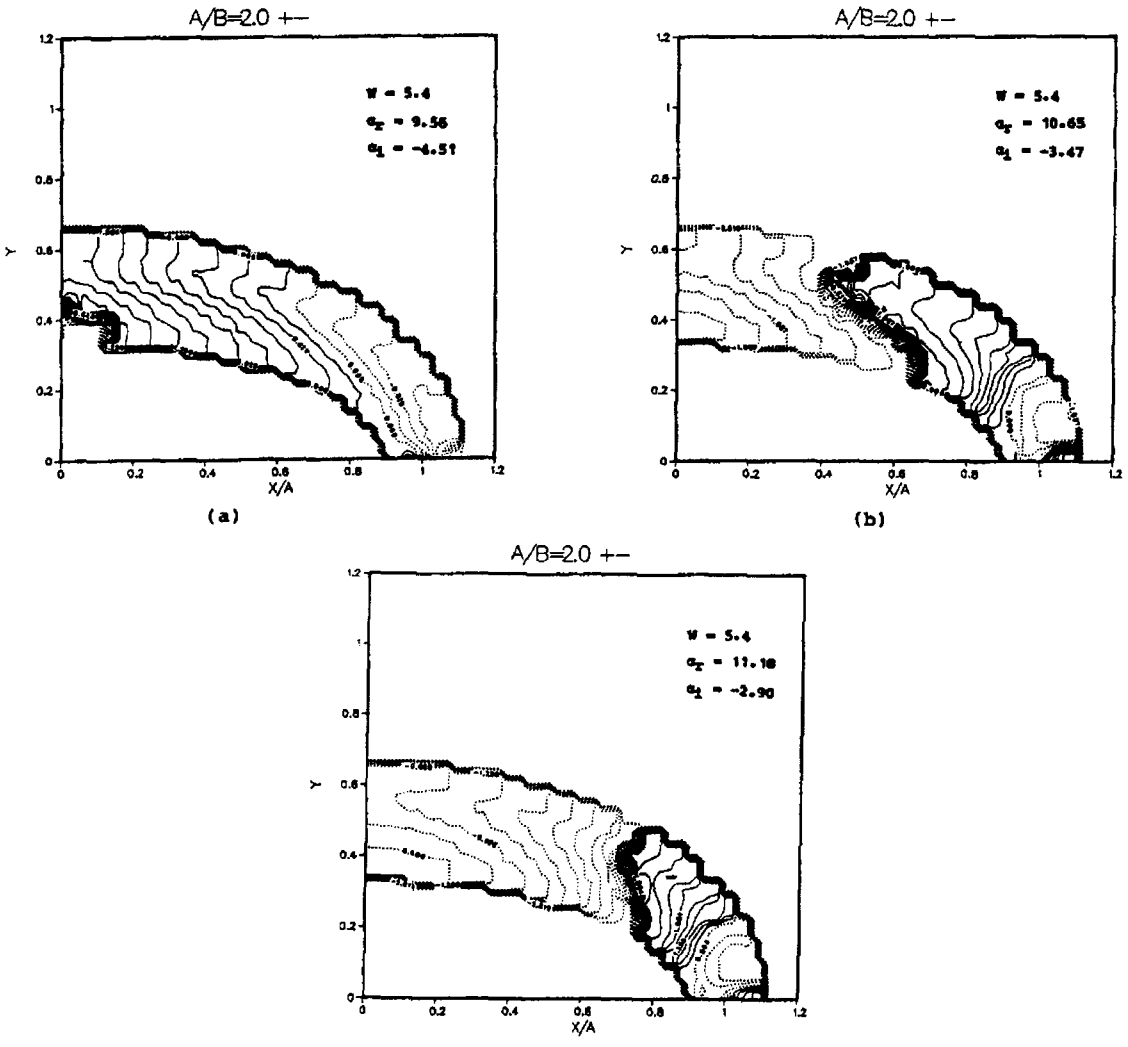

(c)

Figure 12. Phase Variations of the Eigenvectors Corresponding to the Eigenvalues in Figure 10(b) (dotted line = negative, solid line = positive).

5. Summary

The formulation for the mean stability analysis of a compressible heated jet with an arbitrary mean velocity profile has been derived. The application of the formalism to a simpler case showed good agreement with the results of Morris and Miller. In this paper it was not reported that incorporation of viscous effects falls within this formalism very nicely.

And finally, it has been shown that the elliptic jet involves much more complex behavior than the circular case.

6. Acknowledgement

We wish to thank Prof. P. J. Morris for sending us his calculation results. Thanks are also due to Dr. R. L. Derr for his encouragement given to us during the course of this work.

7. References

[1]P. J. Morris, and D. G. Miller. "Wavelike Structures in Elliptic Jets," AIAA Paper 84-0399, 1984.

[2]E. Mollo-Christensen. "Jet Noise and Sheer Flow Instability Seen From an Experimenter's Viewpoint," Trans. A. S. M. E. E., J. Fluid Mech., Vol. 89, pp. 1-7, 1967.

[3]S. C. Crow and F. H. Champagne. "Orderly Structure in Jet Turbulent," J. Fluid Mech.,Vol. 48, pp. 547-591, 1971.

[4]H. V. Fuchs. "Space Correlations of the Fluctuating Pressure in Subsonic Jets," J. Sound Vib., Vol. 22, pp. 77-79, 1972.

[5]A. Michalke. "On Spatially Growing Disturbances in an Inviscid Shear Layer," J. Fluid Mech., Vol. 23, pp. 521-544, 1965.

[6]A. Michalke. "Instability of Compressible Circular Free Jet With Consideration of the Influence of the Jet Boundary Layer Thickness," NASA Tech. Memo 75190, 1977, 1971.

[7]Y. Y. Chan. "Spatial Waves in Turbulent Jets," Phys. Fluids, Vol. 17, pp. 46-53, 1974.

[8]N. Trentacoste and P. N. Sforza. "Further Experimental Results for Three-Dimensional Free Jets," AIAA J., Vol. 5, pp. 885-891, 1967.

[9]Y. Komatsu. "Fluid Dynamics of Jets," Nippon University, Tokyo, Res. Rept., pp. 1-245, 1969.

[10]A. Krothapalli, D. Baganoff, and K. Karamcheti. "On the Mixing of a Rectangular Jet," J. Fluid Mech., Vol. 107, pp. 201-220, 1981.

[11]E. Gutmark and C. M. Ho. "Near-Field Pressure Fluctuations of an Elliptic Jet," AIAA J., Vol. 23, pp. 354-358, 1985.

[12]E. Gutmark, K. C. Schadow, D. M. Parr, C. K. Harris, and K. J. Wilson. "The Mean and Turbulent Structure of Noncircular Jets," AIAA Paper 85-0543, 1985.

[13]D. G. Crighton. "Instability of an Elliptic Jet," J. Fluid Mech., Vol. 59, pp. 665-672, 1973.

[14]D. G. Crighton and M. Gaster. "Stability of Slowly Diverging Jet Flow," J. Fluid Mech., Vol. 77, pp. 397-413, 1976.

[15]P. J. Morris. "The Spatial Viscous Instability of Axisymmetric Jets," J. Fluid Mech., Vol. 77, pp. 511-529, 1976.

[16]S. Koshigoe. "Mathematical Modeling of the Auditory Periphery," Doctoral Dissertation, Purdue University, W. Lafayette, Indiana, 1983. (Available from Xerox University Microfilm, Ann Arbor, Michigan.)

[17]J. R. MacDonald and M. K. Brackman. "Linear-System Integral Transform Relations," Rev. Mod. Phys., Vol. 28, pp. 393-422, 1956.

[18]J. S. Toll. "Causality and Dispersion Relation: Logical Foundations," Phys. Rev., Vol. 104, pp. 1760-1770, 1956.

[19]A. Papoulis. "The Fourier Integral and its Applications," McGraw-Hill, New York, 1962.

[20]S. Koshigoe and A. Tubis. "Implication of Causality, Time-Translation Invariance, Linearity, and Minimum Phase Behavior for Basilar Membrane Response Functions," J. Acoust. Soc. Am., Vol. 71, pp. 1194-1200, 1982.